Research Article

ALWT based Regularizer for Improvement of Low Intensity Visual Data

Jyothula Sunil Kumar[1], T. Jaya Chandra Prasad[2]

[1]Research Scholar, Department of Electronics and Communication Engineering,JNTUA, Anantapur, Andhra Pradesh, India.
[2]Professor, Department of Electronics and Communication Engineering, Rajeev Gandhi Memorial College of Engineering and Technology, Affiliated to JNTUA, Nandyal, Andhra Pradesh, India.

Article History: Received: 10 January 2021; Revised: 12 February 2021; Accepted: 27 March 2021; Published online: 28 April 2021

ABSTRACT

Image Completion is the process of recovering corrupted image with very limited observations. It is a challenging task to achieve accurate recovery in image with minimum observations. Many researchers are proposed various methods to recover the corrupted image. Here a new Adaptive Lifting Wavelet Transform (ALWT) based Alternating Direction Method of Multipliers (ADMM) optimization technique is proposed. A spiffing image recovery is observed at 90% of missing ratio. The non-linear filters are used in ALWT to obtain the lost observations. The Image Quality Assessment (IQA) metrics are considered to evaluate the performance of proposed approach. The IQA metrics namely Mean Square Error (MSE), Peak Signal to Noise Ratio (PSNR) and Structural Similarity (SSIM) are achieved 32.32, 33.04dB and 0.8666 respectively. Here, the Additive White Gaussian Noise (AWGN) with standard deviation 150 is considered. The Mean Absolute Reconstruction Error (MARE), MSE and PSNR values are obtained as 3.176, 12.11 and 37.31dB respectively.

Keywords Adaptive Lifting, Non-Linear Filter, Alternating Direction Method of Multipliers, Mean Absolute Reconstruction Error.

1. Introduction

Image completion is used in many applications such as compressed sensing, pattern recognition and computer vision applications etc., A highly corrupted image may not convey the correct information. Recovering of these images from limited observations is very difficult. To address these problems image completion methods are introduced as rank minimization. The rank minimization is reducing the singular values of the noisy image. The well-known nuclear norm regularizer method maintain as a convex surrogate of the rank function is used for image completion. The singular value thresholding (SVT) is used to minimize the rank function [1]. The truncated nuclear norm regularization based optimization methods are able to minimize the rank efficiently [2]. Here, the difference of the minimum sum of singular values and rank of an image is considered rather than considering total sum of all singular values. It helps in recovery of the lost intensity values efficiently. But the loss of intensity values are more these methods are unable to recover the information.

A transformation based Regularizer named DRM Regularizer [3], which has able to recover the 80% missing ratio in an image. The DCT transformation is utilized along with Accelerated Proximal Gradient Line (APGL) optimization method. Low Rank Matrix Completion method using truncated nuclear norm and Sparse Regularizer (TNN-SR) [4] is another transformation-based optimization method. It is incorporated with DCT and ADMM, to produce the good structure and texture recovery.

The wavelets are exploiting the correlation structure of an image to define sparse approximation [5-7]. Typically space and frequency are localized in correlation structure. The Discrete Wavelet Transform (DWT) most familiar as first-generation wavelets, where the Fourier Transform (FT) is used in space-frequency localization. The second-generation wavelet transformation is introduced without FT, namely Lifting Wavelet Transform (LWT). The LWT features such as custom design, in-place and faster implementations. The LWT has the drawbacks such as fixed filter structure and unable perform smoothing singularity of an image. To overcome these drawbacks the fixed linear filter is replaced with non-linear filters [8].

In this paper, Adaptive Lifting Wavelet Transform (ALWT) based optimization method is introduced to recover accurate image. The ALWT [9-12] has less computational complexity and the high energy compaction compared with the other transform techniques. The optimization method ADMM is utilized with variable splitting.

The paper is organized as follows. section 2 provided with a brief discussion on the previous work done. Section 3 discussion with proposed methodology. Section 4 describes the experimental results and discussion. Finally, Section 5 concludes.

2. Related work

Recovering of an image from the limited observations will be the difficult task. Image Completion problems are addressed by various authors. The Singular Value Thresholding [1] method is solved recovering of pixels in the image by minimizing the rank. The objective function is

$$\hat{I} = \arg\min_{I} \|I\|_* \qquad Subject\ to\ I_\Omega = R_\Omega \tag{1}$$

Yao Hu et al. [2] proposed a method to recover the image by considering minimum number of observations. The image is recovered based on minimum rank of a corrupted image with less number of computations and minimum time. If the missing ratio increases, the recovered image may not have good structure and texture information. The optimization function written as

$$\hat{I} = \min_{I} \|I\|_r + \alpha \|I\|_F^2 \qquad Subject\ to\ P_\Omega(I) = P_\Omega(R) \tag{2}$$

Y Wang et al. [3] proposed a DCT transformation based APGL optimization method to recover the image is blurred when the corrupted observations have more than 80%. The algorithm is able to recover the extreme visuals. To accomplish the work the objective function written as

$$\hat{I} = arg\min_{I}\|I\|_* + \sum_{i=1}^{s}\lambda_i\|I\|_{DCT}^{p_i,q_i} + \frac{\gamma}{2}\|P_\Omega(I) - P_\Omega(R)\|_F^2 \tag{3}$$

D Jing et al. [4] presented low rank matrix completion using truncated nuclear norm and sparse regularized method to deal with highly corrupted images. The DCT is used in ADMM optimization technique. The DCT transformation has high computational complexity and unable to provide the spacio-frequency localization of the image. The optimization function equation is

$$\hat{I} = \min_{I}\|I\|_* - Tr(A_l I B_l) + \lambda\|W\|_1 \tag{4}$$
$$s.t. P_\Omega(I) = P_\Omega(R)\ where\ W = \mathcal{T}(I)$$

The wavelet transforms are playing a crucial role in all the image processing applications. The Wavelet Transforms has the features like less computational complexity and provides the space-frequency localization [5-7]. R.L. Claypoole et al. [9-11] introduced the non-linear filters with lifting to improve the adaptive selection of filter. A few sets of linear filter coefficients are selected for the non-linear selection. J Stepien et al. [12] proposed scale adaptive lifting schemes. The multiresolution levels are modified through soft thresholding and inversely synthesized. The Alternating Direction Method of Multipliers using the Augmented Lagrange Multipliers introduced to deal convex optimization [13,14]. In the following section the proposed ALWT based ADMM optimization approach is discussed.

The contribution of the work:

- Here a new adaptive lifting transform based ADMM optimization technique has been proposed to have a fast and efficient way of finding the missing observations.
- The non-linear filter selection has been considered to predict the optimal values in the corrupted image. These optimal coefficients are effectively utilized in the variable splitting and ADMM process.
- The proposed method experimented with 90 % pepper noise and 50 % gaussian noise. The IQA metrics are shows the proposed approach is outperforms.

3 PROPOSED METHOD

3.1 BASIC AND ADAPTIVE LIFTING

Lifting Wavelet Transforms have three basic operations such as 1) Split 2) Predict 3) Update. These operations are performed iteratively to an image to create detail and wavelet coefficients as shown in fig. 1.

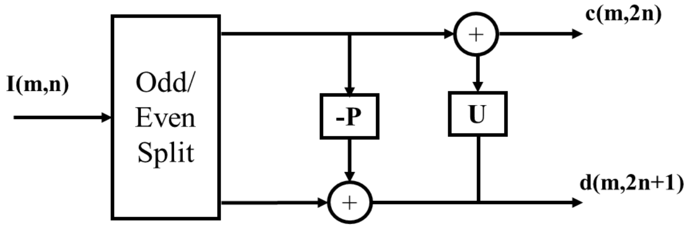

Fig. 1 Basic Lifting Steps

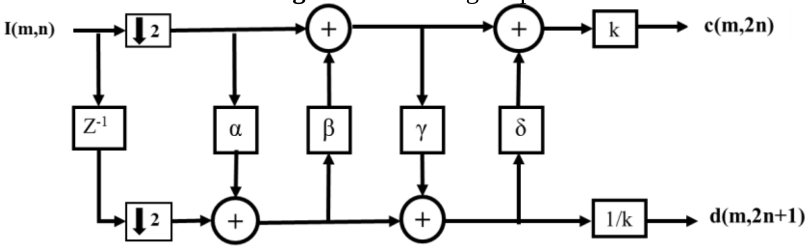

Fig. 2 Lifting 9/7 Wavelet Forward Steps

Split: An image is distributed into two separate subsets $I_e(m, 2n)$ and $I_o(m, 2n + 1)$. $I_e(m, 2n)$ and $Io(m, 2n + 1)$ represents the even indexed points and odd indexed points respectively.

Predict: The detail coefficients are identified as the prediction error between $Ie(m, n)$ and $Io(m, n)$.

$$d[m,n] = I_o[m,2n] - P(I_e[m,n])$$
$$P(I_e[m,n]) = \sum_l p_l I_e[m,n+l] \tag{6}$$

Update: The addition of $I_e[m, n]$ and $d[m, n]$ results the scaling functions $c[m, n]$ as eqn. 7

$$c[m,n] = I_e[m,2n] + P(d[m,n])$$
$$U(d[m,n]) = \sum_k u_k I_e[m,n+k] \tag{7}$$

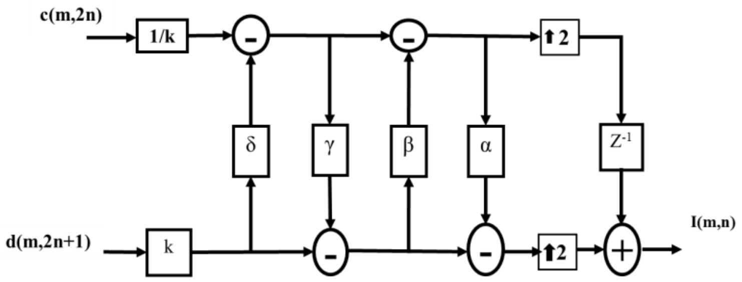

Fig. 3 Lifting 9/7 Wavelet Reverse Steps

The cdf 9/7 and cdf 5/3 bi-orthogonal wavelets are considered for decomposition [15,16]. In fig. 2 and 3 shows the 9/7 wavelet forward and backward process. The Prediction and Updation process are performed based on α, β, γ, and δ. The scaling and wavelet coefficients are calculated by following steps.

$$P1[m,n] = I_o[m,n] + \alpha.*\,(\,I_e[m,n] + I_e[m,n+1])$$
$$U1[m,n] = I_e[m,n] + \beta.*\,(\,P1[m,n] + P1[m,n-1]) \tag{7}$$
$$P2[m,n] = P1[m,n] + \gamma.*\,(\,U1[m,n] + U1[m,n+1])$$
$$U2[m,n] = U1[m,n] + \delta.*\,(\,P2[m,n] + P2[m,n-1]) \tag{8}$$
$$d[m,n] = P2./k$$
$$c[m,n] = k.*\,U2 \tag{9}$$

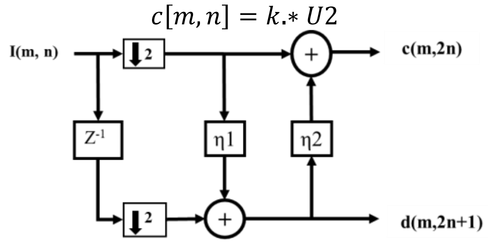

Fig 4 Lifting 5/3 Wavelet Process

The cdf 5/3 wavelet decomposition are performed with two weighing parameters η1 and η2 as shown in fig. 4. The scaling and wavelet coefficients are evaluated by eqn. 10.

$$d[m,n] = I_o[m,n] - \eta 1(I_e[m,n]) + I_e[m,n+1])$$
$$c[m,n] = I_e[m,n] + \eta 2(d[m,n-1], d[m,n]) \tag{10}$$

In Adaptive Lifting Scheme, the Predictor and Update operations are selected at each individual decomposition level. The optimal values are calculated to match the local properties of an image. The Predictor gives the detail coefficients set, among these the lowest energy coefficients are identified as optimal prediction set. After fixing the Predictor coefficients, Updater identifies the approximation coefficients which similar to the original image. These coefficients will be replacing the distorted observations.

3.2 ADAPTIVE LIFTING BASED ADMM

To solve eqn 4. an iterative approach alternating between two steps is proposed by J Dong [4]. The singular value decomposition (SVD) is applied to fix I_l. The SVD gives a diagonal coefficient set and two complex unitary coefficients sets. A_l and B_l are formed by using the identified complex unitary coefficients. Second step I_l is updated by using the A_l and B_l. The optimization function is formed as

$$\widehat{I_{k+1}} = \arg\min_{I} \|I\|_* - Tr\left(A_l I B_l{}^T\right) + \lambda\|N\|_1 \tag{11}$$
$$s.t. P_\Omega(I) = P_\Omega(R)\ where\ N = \mathcal{T}(I)$$

The I will be replaced with $\boldsymbol{\mathcal{M}}$ in the trace term, then the objective function formed as

$$\widehat{I_{k+1}} = \arg\min_{I} \|I\|_* - Tr\left(A_l \mathcal{M} B_l{}^T\right) + \lambda\|N\|_1 \tag{12}$$
$$s.t. P_\Omega(I) = P_\Omega(R)\ where\ N = \mathcal{T}(I)$$

$\mathcal{T}$ represents the transform operator. The ALWT is introduced with the two different filters namely cdf 9/7 and cdf 5/3, to classify the image's best similitude coefficients as described in section 3.1. These coefficients are identified and replaced with the eqn. (12) given the better-quality image. The eqn. (12) solving procedure is summarized in algorithm.

Algorithm: ***ALWT based Regularizer for Visual Recovery***

Observation: *Received image I, Estimation O;*

Input: $\lambda, \varepsilon, r, wname, dlevel, \alpha, \beta, \gamma, \delta, \zeta, \eta 1, \eta 2;$

Initialization: $\mathcal{M} = I_1, N = null\ set, P = I_1;$

$$I_{k+1} = \arg\min_{I} \|I\|_* + \frac{\zeta}{2}\left\| I_k - \frac{1}{2}(\mathcal{M}_k - \frac{O_k}{\zeta} + G(N_k + \frac{P_k}{\zeta} \right\|_F^2$$

Where G(.) performs the inverse transform.

$$\mathcal{M}_{k+1} = I_{k+1} - \frac{O_k}{\zeta} + \frac{A_l^T B_l^T}{\zeta}$$

$$N_{k+1} = \arg\min_{N} \|N\| + \frac{\zeta}{2}\left\|N - H(I_k) + \frac{P}{\zeta}\right\|_F^2$$

Where G(.) performs the forward transform.

$O_{k+1} = O_k + \zeta(\mathcal{M}_{k+1} - I_{k+1})$

$P_{k+1} = P_k + \zeta(N_{k+1} - H(I_{k+1}))$

$k=k+1$

$\boldsymbol{Until}\ \|I_{k+1} - I_k\|_F \leq \epsilon$

$\boldsymbol{Output}: The\ recovered\ image\ \hat{I} = I_{k+1}$

4 RESULTS AND DISCUSSION

Experimental Setup: The system with i3 processor, 8GB RAM and MATLAB 2018a is used to execute the program. The images data set taken from the Laboratory for Image and Video Engineering of The University of Texas at Austin [17]. These images of size 256 × 256. Some of the images (Flower, Parrot, Pepper, Toco, Scenes) are shown in fig. 5. The Tab. 1. describes the parameters are used [15].

Fig. 5 Sample Images considered for testing

Tab. 1 Parameters Used

Parameter	Value
α	-1.586134342
β	-0.052980118
γ	0.882911075
δ	0.443506852
k	1.149604398
η1	-0.5
η2	0.25
λ	0.001
ζ	0.0001

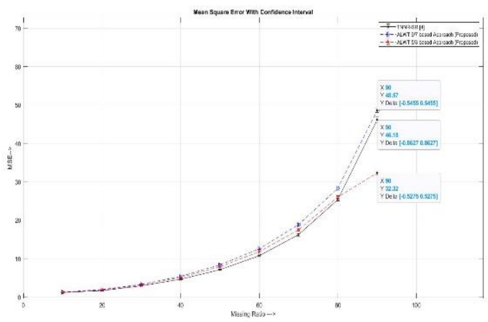

Fig. 6 (a) MSE vs percentage of missing ratio

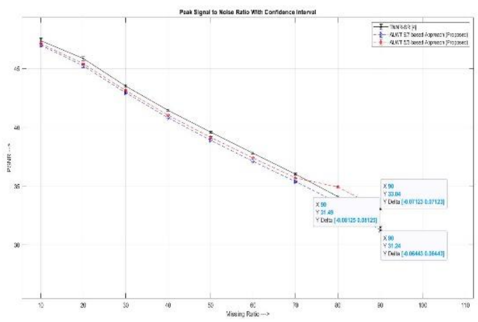

Fig. 6 (b) PSNR vs percentage of missing ratio

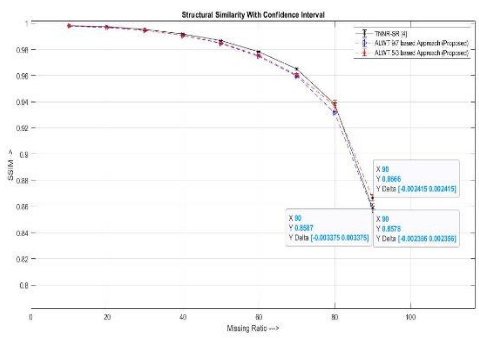

Fig. 6 (c) SSIM vs percentage of missing ratio

Fig. 6 Experimental FR-IQA measures Confidence Interval to Toco recovered image with Missing ratios varies from 10% to 90% (Pepper Noise)

The typical evaluation metrics Full Reference Image Quality Assessment (FR-IQA) and No-Reference Image Quality Assessment (NR-IQA) are used. FR-IQA measures MSE, PSNR, and SSIM are calculated and shown in fig. 6. NR-IQA measures Blind / No-Reference Image Spatial Quality Evaluator (BRISQUE) [18], Natural Image Quality Evaluator (NIQE) [19], and Perceptual Image Quality Evaluator (PIQE)[20] are calculated and presented in the fig. 7.

MARE: The Mean Absolute Reconstruction Error (MARE) of original image to the reconstructed image can be written as

$$MARE = \frac{1}{m * n * p} \sum_{k}^{p} \sum_{j}^{n} \sum_{i}^{m} \left| I_{ijk} - \hat{I}_{ijk} \right| \tag{13}$$

PSNR: The FR-IQA measure PSNR is considered to evaluate the results. The following equation is used to evaluate

$$PSNR = 10 \ \log_{10} \frac{255^2}{MSE}$$

The fig. 6 shows the experimental results of the image missing observations ranging from 10% to 90% missing ratio. The performance of proposed ALWT based ADMM is compared with existing method proposed by D Jing [4]. The ALWT based ADMM approach is considered with two different wavelet decomposition methods named cdf 9/7 and cdf 5/3. The ALWT based ADMM with 5=3 wavelet decomposition is obtained minimum MSE, high PSNR and SSIM Values as 32.32, 33.04dB and 0.8666 respectively. In fig. 6(a), 6(b) and 6(c) the metrics MSE, PSNR, and SSIM are plotted with 10% to 90% missing ratios respectively.

The ALWT53ADMM has the minimum MSE value from 70% missing ratio on-wards it gives the maximum PSNR Value. The optimal missing values are identified using the horizontal and vertical prediction of lifting scheme. The lifting filter cdf 5/3 has less computations compared with the cdf 9/7. The time required to reach optimal value becomes less. The predicted optimal value will be updated by using the updater process.

The confidence interval for the pepper noise ranging from 10% to 90% is shown in fig 6. The FR-IQA measures and the NR-IQA measures are calculated confidence interval using the Z-Distribution. To 90% missing entries images are recovered with the proposed approach provided the 99% of PSNR confidence interval as 33.04 ± 0.07123. The SSIM confidence interval is 0.8666 ± 0.002415. In fig. 7 the NR-IQA measures BRISQUE, NIQE, and PIQE. The minimal values of NR-IQA indicates the good recovery. Here the fig. 7(a) shows the BRISQUE metric providing the high score for good recovered image. An image recovered from less corrupted image has good visual quality, but the BRISQUE score is high. The NIQE metric gives the better scores for all the cases as shown in fig. 7(b). The missing ratio of 90% the NIQE scored as 9.692. To existing approach the NIQE scored as 10.25 ± for the %90 missing ratio. From the fig. 7(c) it is observed that the PIQE metric also providing the high scores for the visually better recovered images for lower missing ratios. The measures of recovered image using the proposed methods scored minimal values as compared with TNNR-SR [4]. Fig 7(d) shows the time taken to recover the various missing ratios (ranges from 10% missing ratio to 90% missing ratio) of the image. To higher

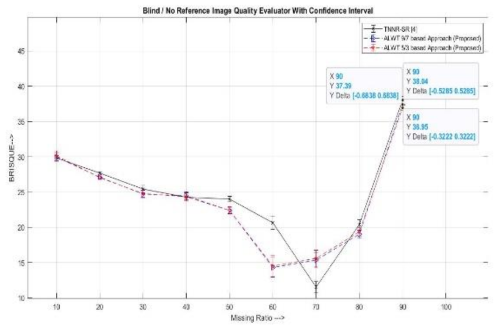

Fig. 7 (a) BRISQUE vs Missing ratio

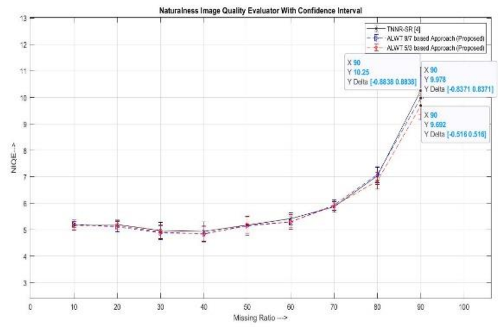

Fig. 7 (b) NIQE vs Missing ratio

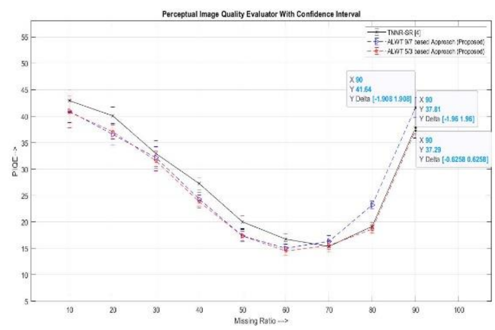

Fig. 7 (c) PIQE vs Missing ratio

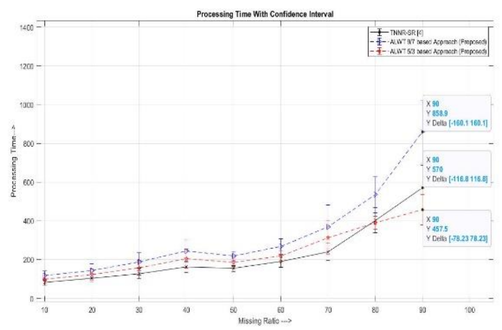

Fig. 7 (d) Processing Time vs Missing ratio

Fig. 7 Experimental NR-IQA measures Confidence Interval to Toco recovered image with Missing ratios varies from 10% to 90 %

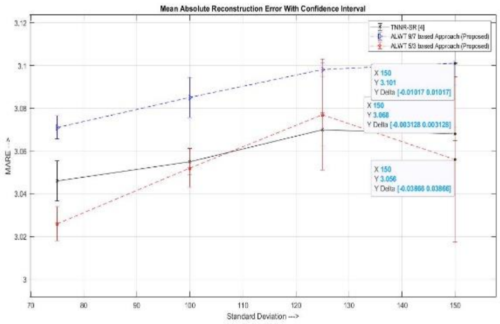

Fig. 8 (a) MARE VS Standard Deviation

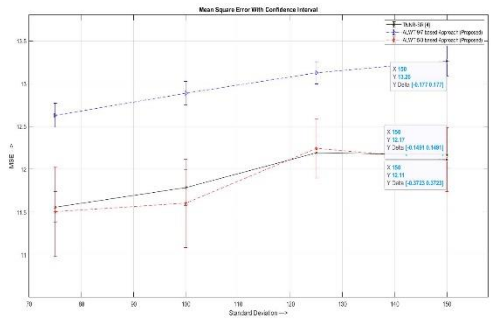

Fig 8 (b) MSE vs Standard Deviation

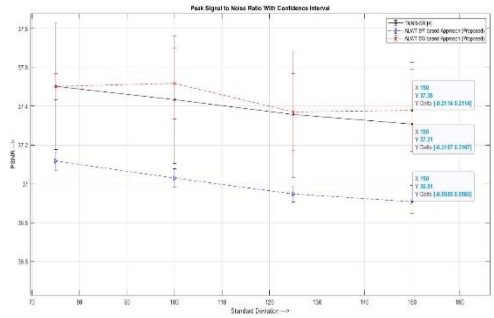

Fig. 8 (c) PSNR vs Standard Deviation

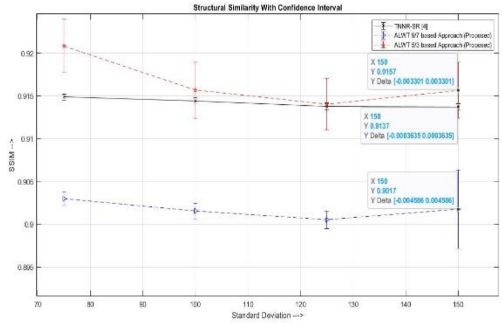

Fig. 8 (d) SSIM vs Standard Deviation

Fig. 8 Experimental FR-IQA measures Confidence Interval to Toco recovered image with 50 percent additive gaussian noise with zero mean and 150 standard deviation

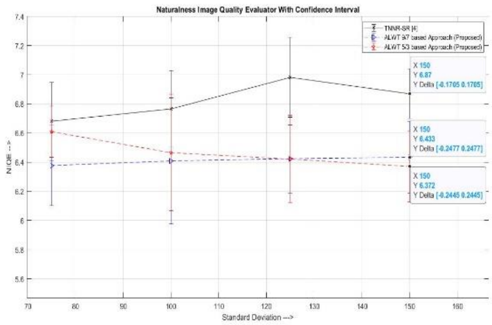

Fig. 9 (a) BRISQUE vs Standard Deviation

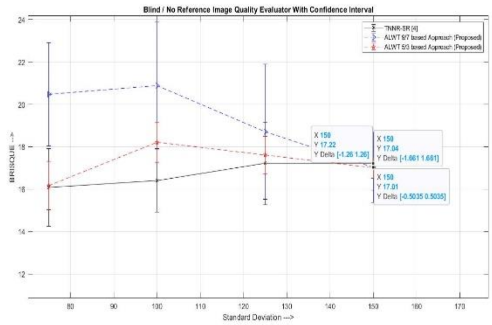

Fig. 9 (b) NIQE vs Standard Deviation

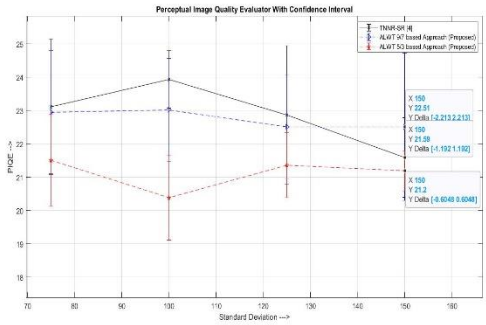

Fig. 9 (c) PIQE vs Standard Deviation

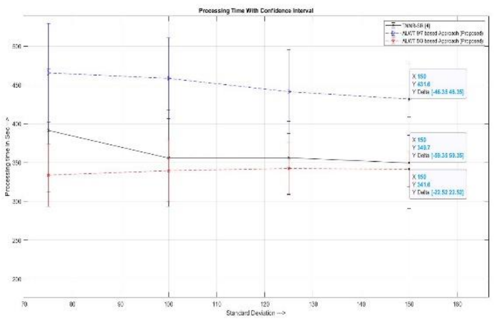

Fig. 9 (d) Processing Time vs Standard Deviation

Fig. 9 Experimental NR-IQA measures Confidence Interval to Toco recovered image with 50 percent additive gaussian noise with zero mean and 150 standard deviation

missing ratios the proposed approach provided the good recovery and less time. The NR-IQA measures BRISQUE, NIQE and PIQE confidence interval values are 36.95±0.3222, 9.672±0.516, and 37.29±0.6258 respectively. The time taken to recover confidence interval is 457.5±78.23 to the ALWT53ADMM approach.

Fig. 8 shows the recovered image from gaussian noise with 70 to 150 standard deviation values. The MARE, MSE and PSNR values obtained as 3.056, 12.11 and 37.31dB respectively to the standard deviation 150. The proposed adaptive lifting based optimization approach is able to predict the optimal missing values. The NR-IQA measures BRISQUE, NIQE, PIQE and Processing time are plotted in fig. 9. The results are stating that the proposed ALWT53ADMM is recovered as similar to the existing approach. The time taken to recover from gaussian noise is 341.6 seconds which is smaller than the existing methods.

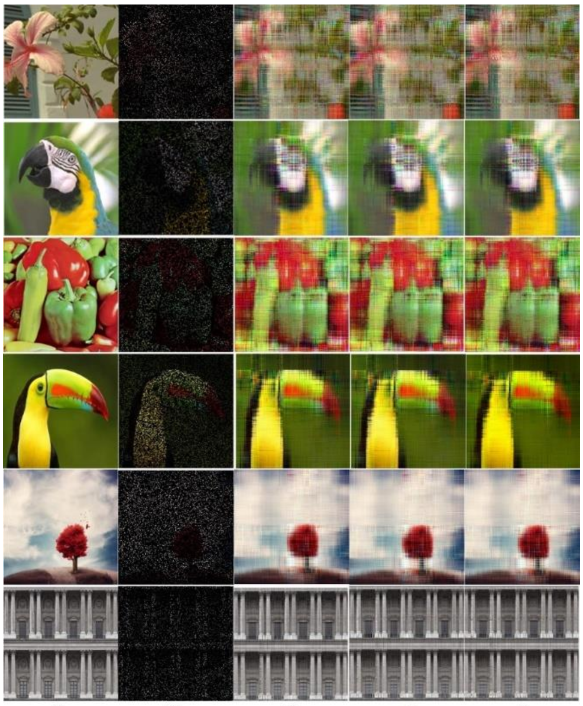

Fig. 10. Recovered images from 90 Percent missing ratio (Pepper Noise), a) Original Images, b) Noise added images, c) TNNR-SR (Existing Approach), d) Adaptive 9/7 Lifting based ADMM, and e) Adaptive 5/3 Lifting based ADMM (Proposed approach)

The results of recovered images using existing and proposed methods are presented in fig. 10 (recovered from 90 % pepper noise) and fig. 11(recovered from 50% Additive Gaussian Noise Gaussian noise).

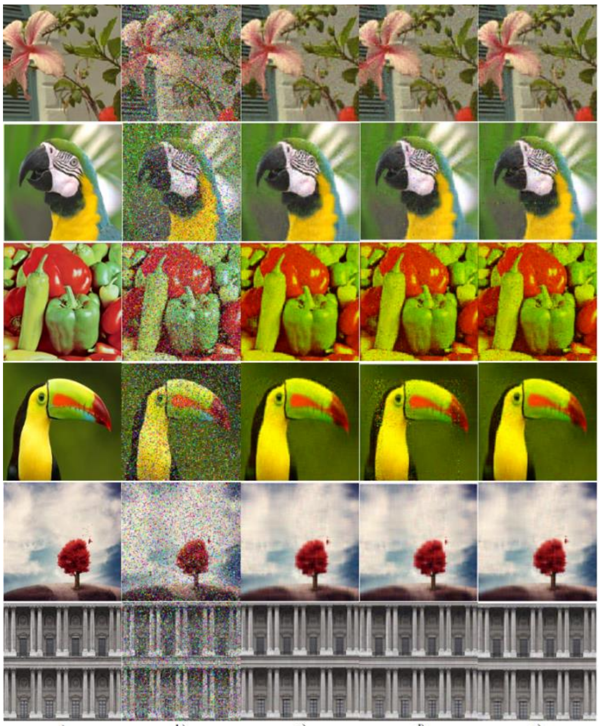

Fig. 11. Recovered images from 50 Percent Additive Gaussian Noise with standard deviation 150, a) Original Images, b) Noise added images, c) TNNR-SR (Existing Approach), d) Adaptive 9/7 Lifting based ADMM, and e) Adaptive 5/3 Lifting based ADMM (Proposed approach)

The consolidated metrics with confidence interval are tabulated in Tab. 2 and 3. The Tab. 2 provided with the 90% missing ratio (Pepper Noise) recovered image and Tab. 3 III provided the recovered image IQA metrics from 50% Additive Gaussian Noise.

Tab. 2 IQA measures of Recovered Image from 90% missing ratio (Pepper Noise)

Random Pepper Noise of 90%			
Metric	**Existing Approach**	**Proposed Approach**	
	TNNR-SR	**ALWT97ADMM**	**ALWT53ADMM**

MSE	46.18±0.8627	48.87±0.7324	32.32±0.5275
PSNR (dB)	31.49±0.08125	31.24±0.06443	33.04 ±0.07123
SSIM	0.8578±0.002356	0.8587±0.003375	0.8666 ±0.002415
BRISQUE	38.04±0.5285	37.39±0.6838	36.95±0.3222
NIQE	10.25±0.8838	9.978±0.8371	9.692±0.516
PIQE	37.81±1.96	41.64±1.908	37.29±0.6258
Processing Time (sec)	570±116.8	858.9±160.1	457.5±78.23

Tab. 3 IQA measures of Recovered Image from 50% Additive Gaussian Noise

Random Additive Gaussian Noise of 50% with 150 Standard Deviation			
Metric	**Existing Approach**	**Proposed Approach**	
	TNNR-SR	**ALWT97ADMM**	**ALWT53ADMM**
MARE	3.068±0.003128	3.103±0.01109	3.056±0.03866
MSE	12.17±0.1491	13.26±0.177	12.11±0.3723
PSNR (dB)	37.28±0.05336	36.91±0.0585	37.31±0.3167
SSIM	0.9137±0.0003635	0.9017±0.004586	0.9157±0.003301
BRISQUE	17.22±1.26	17.04±1.661	17.01±0.5032
NIQE	6.87±0.1705	6.433±.02477	6.372±0.2445
PIQE	21.59±1.192	22.51±2.213	22.4±1.375
Processing Time (sec)	349.7±59.35	431.6±46.35	341.6±22.52

5 Conclusions

The proposed approach ALWT based ADMM is tested with the two different noises. Initially, An image with 90 % of pepper noise corrupted observations, the proposed model is obtained the MSE and PSNR confidence interval values as 32.32±0.5275 and 33.04 ± 0.07123dB respectively and the MSE value is decreased by 39.87%. The PSNR is increased by 7.04%. The processing time taken as 457.5±78.23 seconds. Secondly, the Additive Gaussian noise of 50 percent with the standard deviation 150, the MARE, MSE and PSNR values as 3.056±0.03866, 12.11±0.3723 and 37.31±0.3167dB respectively to the standard deviation 150. The gaussian noise corrupted image processing time is 341.6±22.52 seconds. The results are concluding that the proposed process is performing the better reconstruction of an image in both the noises.

References

1. Jian-Feng Cai, Emmanuel J Cand`es, and Zuowei Shen. A singular value thresholding algorithm for matrix completion. SIAM Journal on optimization, 20(4):1956-1982, 2010.
2. Yao Hu, Debing Zhang, Jieping Ye, Xuelong Li, and Xiaofei He. Fast and accurate matrix completion via truncated nuclear norm regularization. IEEE transactions on pattern analysis and machine intelligence, 35(9):2117-2130, 2012.
3. Yunhe Wang, Chang Xu, Shan You, Chao Xu, and Dacheng Tao. DCT regularized extreme visual recovery. IEEE Transactions on Image Processing, 26(7):3360-3371, 2017.
4. Jing Dong, Zhichao Xue, Jian Guan, Zi-Fa Han, and Wenwu Wang. Low rank matrix completion using truncated nuclear norm and sparse regularizer. Signal Processing: Image Communication, 68:76-87, 2018.
5. Ingrid Daubechies and Wim Sweldens. Factoring wavelet transforms into lifting steps. Journal of Fourier analysis and applications, 4(3):247-269, 1998.
6. Wim Sweldens. The lifting scheme: A custom-design construction of biorthogonal wavelets. Applied and computational harmonic analysis, 3(2):186-200, 1996.
7. Wim Sweldens. The lifting scheme: A construction of second-generation wavelets. SIAM journal on mathematical analysis, 29(2):511-546, 1998.
8. Zhi-Zhong Han, Zhen-Bao Liu, and Ya-Sen Xu. A new adaptive wavelet transform using lifting scheme. In 2011 International Conference on Wavelet Analysis and Pattern Recognition, pages 224-229. IEEE, 2011.
9. Roger L Claypoole, Geoffrey M Davis, Wim Sweldens, and Richard G Baraniuk. Nonlinear wavelet transforms for image coding via lifting. IEEE Transactions on Image Processing, 12(12):1449-1459, 2003.
10. Roger L Claypoole, Richard G Baraniuk, and Robert D Nowak. Adaptive wavelet transforms via lifting. In Proceedings of the 1998 IEEE International Conference on Acoustics, Speech and Signal Processing, ICASSP'98 (Cat. No. 98CH36181), volume 3, pages 1513-1516. IEEE, 1998.

11. Roger L Claypoole, Richard G Baraniuk, and Robert David Nowak. Lifting construction of non-linear wavelet transforms. In Proceedings of the IEEE-SP International Symposium on Time-Frequency and Time-Scale Analysis (Cat. No. 98TH8380), pages 49-52. IEEE, 1998.
12. Jacek Stepien, Tomasz Zielinski, and Roman Rumian. Image denoising using scaleadaptive lifting schemes. In Proceedings 2000 International Conference on Image Processing (Cat. No. 00CH37101), volume 3, pages 288-291. IEEE, 2000.
13. Stephen Boyd, Neal Parikh, Eric Chu, Borja Peleato, and Jonathan Eckstein. Distributed optimization and statistical learning via the alternating direction method of multipliers. Foundations and Trends R in Machine learning, 3(1):1-122, 2011.
14. Zhouchen Lin, Minming Chen, and Yi Ma. The augmented lagrange multiplier method for exact recovery of corrupted low-rank matrices. arXiv preprint arXiv:1009.5055, 2010.
15. Sanjay H Dabhole, Virajit A Gundale, and Johan Potgieter. An efficient modified structure of cdf 9/7 wavelet based on adaptive lifting with spiht for lossy to lossless image compression. In 2013 International Conference on Signal Processing, Image Processing & Pattern Recognition, pages 269-274. IEEE, 2013.
16. Andreas E Savakis and Richard Carbone. Discrete wavelet transform core for image processing applications. In Real-Time Imaging IX, volume 5671, pages 142-151. International Society for Optics and Photonics, 2005.
17. HR Sheikh. Live image quality assessment database release 2. http://live. ece. utexas.edu/research/quality, 2005.
18. Anish Mittal, Anush Krishna Moorthy, and Alan Conrad Bovik. No-reference image quality assessment in the spatial domain. IEEE Transactions on image processing, 21(12):4695-4708, 2012.
19. Anish Mittal, Rajiv Soundararajan, and Alan C Bovik. Making a \completely blind" image quality analyzer. IEEE Signal Processing Letters, 20(3):209-212, 2012.
20. N Venkatanath, D Praneeth, Maruthi Chandrasekhar Bh, Sumohana S Channappayya, and Swarup S Medasani. Blind image quality evaluation using perception based features. In 2015 Twenty First National Conference on Communications (NCC), pages 1-6. IEEE, 2015.